

Optical probes of coherence in two dimensional Bose gases of polaritons

Joseph Jachinowski*

James Franck Institute and the Department of Physics, University of Chicago, Chicago, IL 60637, USA

Hassan Alnatah and David W. Snoke

*Department of Physics, University of Pittsburgh,
3941 O'Hara Street, Pittsburgh, Pennsylvania 15218, USA*

Peter B. Littlewood

*James Franck Institute and the Department of Physics,
University of Chicago, Chicago, IL 60637, USA and
School of Physics and Astronomy, University of St Andrews, St Andrews KY16 9SS, United Kingdom*
(Dated: March 12, 2025)

Due to their photonic components, exciton-polariton systems provide a convenient platform to study the coherence properties of weakly-interacting Bose gases and the Bose-Einstein condensate transition. In particular, optical interferometry enables the measurement of the first-order coherence function which provides insight into the phase of the system. In this paper, we analyze the buildup of coherence in finite-sized, noninteracting, equilibrium Bose gases through the condensate fraction and the related coherent fraction, defined via the first-order coherence function. Our results provide a baseline to compare against experimental data. Discrepancies may indicate where interacting or nonequilibrium models are necessary to describe the system. In the normal phase, before the Bose-Einstein condensate transition, Bose gases exhibit partial spatial and temporal coherence. This significantly alters the paraxial propagation and interference of optical signals from exciton-polariton systems. Therefore, we also analyze diffraction related to the introduction of apertures and time-delay between interferometry arms, given the partial coherence of the source. Comparison to experiment shows remarkable agreement with the noninteracting Bose gas theory, even approaching the quasi-condensate regime.

I. INTRODUCTION

Exciton-polaritons (EP) are bosonic matter-light quasiparticles formed by coupling excitons, bound electron-hole pairs in solids, to photons confined in optical cavities [1, 2]. While the excitonic component endows the EPs with interactions, the photonic component keeps the effective mass very small and the particles delocalized, driving the Bose-Einstein condensate (BEC) transition from cryogenic temperatures up towards room temperature.

Various experiments have investigated the signatures of BEC in EP systems [3–6]. But besides BEC, EPs systems possess a wide range of accessible phases [7] due their multicomponent driven-dissipative nature. Such phases can be probed by measuring the first-order coherence function, and experiments have confirmed the buildup of (quasi)-long-range-order near a critical pump power [8] [9] and the spontaneous formation of quantized vortices [10] related to superfluidity.

While, in principle, nonequilibrium pumping and decay processes complicate the system, it is possible to prepare EP samples which are well-described by the equilibrium Bose-Einstein distribution [11]. Our paper is mostly concerned with understanding this limit as a baseline for comparison. Outside of this regime, other experiments

have explored the phenomena of multimode condensation [12] as well as the Berezinskii-Kosterlitz-Thouless (BKT) phase [13, 14] in a nonequilibrium setting [15] and its interplay with Kardar-Parisi-Zhang (KPZ) physics [16–18].

In this paper, we discuss some general aspects of coherence measurements in finite-sized, two dimensional Bose gases; in particular, we focus on how coherence builds up as the density approaches the critical density. The brunt of our analysis is based on the first-order coherence function for a noninteracting, equilibrium Bose gas of EP which we use to define the condensate fraction and the coherent fraction measured in interferometry experiments. Since EP systems are monitored by collimated optical signals, the finite-size is imposed as a Gaussian beam profile or a finite aperture. The theory of partial coherence in optics allows us to study the paraxial propagation of the signal and subsequent corrections to the measured coherence. Apertures are generally introduced into an imaging system in order to limit the effects of EP sample inhomogeneities which are a result of microcavity disorder or pump beam aberrations. As a motivating example, a recent experiment Ref. [19] used an aperture before measuring the first-order coherence function via a Michelson interferometer.

Our principal result is the functional behavior of the coherent fraction (defined in Sec. II C) with the system parameters, most importantly the temperature, particle number, and aperture radius. In particular, we do not find power-law behavior with the particle number, but

* jachinowski@uchicago.edu

instead steep growth which looks approximately like a power-law over a limited range of particle numbers near the BEC transition. We conclude with a discussion of the limitations of our results to weakly-interacting, equilibrium gases. In Ref. [19], they simulate their experiment with the Gross-Pitaevskii equation and find good agreement in the low-density regime, though without any analytic context. We further analyze this experiment in light of our analytic calculations and present a comparison to the experiment in Fig. 4. We find good agreement away from the BEC transition to a model with no free parameters thus constraining future studies. Our results are broadly applicable to optical interference experiments with partially coherent sources.

II. THEORY OF COHERENCE IN BOSE GASES

A. First-order coherence functions

In this section, we review the microscopic description of the EP system and discuss some general aspects of first-order coherence functions in Bose gases. The Hamiltonian for a gas of (lower) EPs in second-quantized form is

$$H = \sum_{\mathbf{k}_{\parallel}} \epsilon(\mathbf{k}_{\parallel}) P_{\mathbf{k}_{\parallel}}^{\dagger} P_{\mathbf{k}_{\parallel}} \quad (1)$$

where \mathbf{k}_{\parallel} is the in-plane component of the EP momentum perpendicular to the cavity axis, $\epsilon(\mathbf{k}_{\parallel})$ is the in-plane EP dispersion, and $P_{\mathbf{k}_{\parallel}} = A_{\mathbf{k}_{\parallel}} a_{\mathbf{k}_{\parallel}} + B_{\mathbf{k}_{\parallel}} b_{\mathbf{k}_{\parallel}}$ is the EP annihilation operator constructed from the photon annihilation operator $a_{\mathbf{k}_{\parallel}}$, exciton annihilation operator $b_{\mathbf{k}_{\parallel}}$, and Hopfield coefficients $A_{\mathbf{k}_{\parallel}}$ and $B_{\mathbf{k}_{\parallel}}$ which depend on the cavity detuning and the exciton-photon coupling. Since cavity photons have finite lifetimes, the EP wavefunction is accessible as a projection onto the escaped photons $a_{\mathbf{k}_{\parallel}}$. The (equal-time) first-order coherence function $G^{(1)}$ of the EPs is then

$$\begin{aligned} G^{(1)}(\mathbf{r}, \mathbf{r}') &= \langle \Psi^{\dagger}(\mathbf{r}) \Psi(\mathbf{r}') \rangle \\ &= \int \frac{d^2 k_{\parallel}}{(2\pi)^2} e^{i\mathbf{k}_{\parallel} \cdot (\mathbf{r} - \mathbf{r}')} \langle a_{\mathbf{k}_{\parallel}}^{\dagger} a_{\mathbf{k}_{\parallel}} \rangle \end{aligned} \quad (2)$$

where \mathbf{r} and \mathbf{r}' are positions in the plane perpendicular to the cavity axis, $\Psi(\mathbf{r})$ is the field operator associated with the photon mode annihilation operator $a_{\mathbf{k}_{\parallel}}$ calculated via Fourier transform, and the second equality is the well-known relation between the first-order coherence function for a noninteracting, homogeneous system and the momentum distribution $\tilde{n}(\mathbf{k}_{\parallel}) = \langle a_{\mathbf{k}_{\parallel}}^{\dagger} a_{\mathbf{k}_{\parallel}} \rangle$. For an equilibrium Bose gas in the grand canonical ensemble, we use the Bose-Einstein momentum distribution $\tilde{n}(\mathbf{k}_{\parallel}) = \left(z^{-1} e^{\lambda_T^2 k_{\parallel}^2 / 4\pi} - 1 \right)^{-1}$. The relevant parameters are the fugacity $z = e^{\mu/k_B T}$ expressed in terms of

the chemical potential μ , the temperature T , and Boltzmann's constant k_B , and the thermal de Broglie wavelength $\lambda_T = \sqrt{2\pi\hbar^2/mk_B T}$ where m is the EP mass and \hbar is the reduced Planck constant.

In general, the first-order coherence function can be calculated as a power series in the fugacity using only the single-particle propagator [20]. For a homogeneous system in two dimensions, like the EP system, the result is

$$G^{(1)}(\mathbf{r}, \mathbf{r}') = \frac{1}{\lambda_T^2} \sum_{j=1}^{\infty} \frac{z^j}{j} e^{-\pi(\mathbf{r}-\mathbf{r}')^2/j\lambda_T^2} \quad (4)$$

The first-order coherence function can be normalized by the (homogeneous) density $n = G^{(1)}(\mathbf{r}, \mathbf{r}) = -\log(1-z)/\lambda_T^2$. The resulting (equal-time) normalized first-order coherence function $g^{(1)}(\mathbf{r}, \mathbf{r}')$ is plotted in Fig. 1a for various fugacities. In the classical Maxwell-Boltzmann limit $z \rightarrow 0$, the standard result of a Gaussian first-order coherence function with classical coherence length $\xi_0 = \lambda_T/\sqrt{\pi}$ is obtained. In the following, we use ‘‘Bose gas correlations’’ to refer to a system with a finite fugacity and first-order coherence function given by Eq. 4.

For a finite fugacity, the first-order coherence function is non-Gaussian. However for small fugacities $z \ll 1$ it is useful to consider an effective Gaussian shape characterized by an effective coherence length ξ_{eff} [21]. Fixing the temperature and hence ξ_0 , we fit a Gaussian to the short-range portion of the exact first-order coherence function Eq. 4 and numerically find that ξ_{eff} grows linearly with the density in the regime $z \ll 1$. An example fit for $z = 0.2$ is shown in Fig. 1a. The deviation of the exact first-order coherence function from the Gaussian form becomes more prominent as the fugacity increases. Details on the long-range behavior of the first-order coherence function can be found in Appendix A. We will be primarily concerned with the $z \rightarrow 1$ limit where the effective Gaussian approximation does not apply.

The time-correlations can be studied in a similar manner to Eq. 4 after generalizing the definition of the first-order coherence function Eq. 2 to finite time-separations $t - t'$. Following Ref. [22], the (equal-position) first-order coherence function for a homogeneous system in two dimensions can be expressed in terms of the Lerch transcendent. Defining the dimensionless thermal time-separation $\theta = k_B T(t - t')/\hbar$, in the limit $\theta \gg 1$ the asymptotic expansion of the Lerch transcendent [23] yields correlations which go as

$$G^{(1)}(\theta) \sim \frac{1}{\lambda_T^2} \frac{z}{1-z} \frac{e^{-i \tan^{-1}(\theta)}}{\sqrt{1+\theta^2}} \quad (5)$$

The (equal-position) normalized first-order coherence function $g^{(1)}(t, t')$ is plotted in Fig. 1b for various fugacities. The characteristic time-scale of the decay depends strongly on the fugacity z and, consequently, the

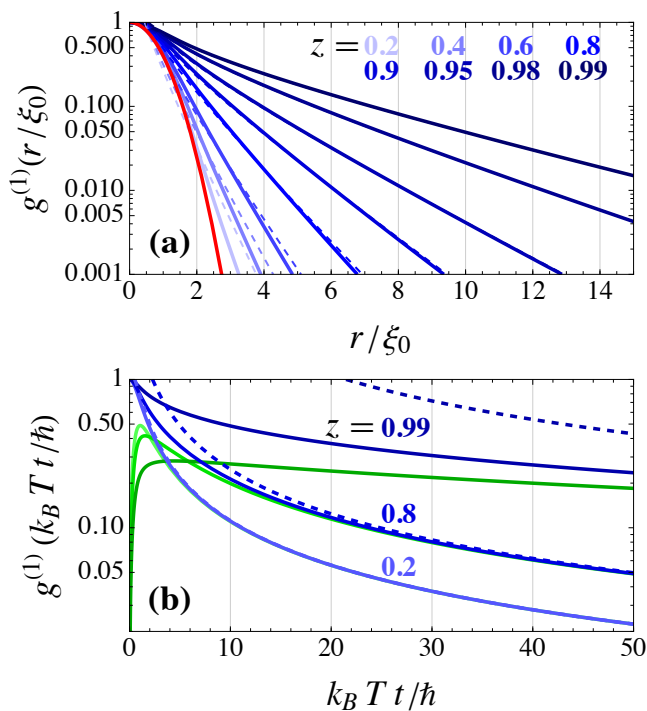


FIG. 1. Correlations of a noninteracting, homogeneous Bose gas in two dimensions. (a) Exact (solid blue) and asymptotic (dashed blue) equal-time normalized first-order coherence function $g^{(1)}$ as a function of the normalized separation r/ξ_0 where $\xi_0 = \lambda_T/\sqrt{\pi}$ is the classical coherence length. (Solid red) Short-range Gaussian fit of the exact $z = 0.2$ first-order coherence function. The width of the effective Gaussian correlations grows linearly with the density for $z \ll 1$ (see text). (b) Exact (solid blue) and asymptotic (dashed blue) equal-position normalized first-order coherence function magnitude $|g^{(1)}|$ as a function of the dimensionless thermal time-separation $\theta = k_B T t / \hbar$. (Solid green) Imaginary part of the equal-position normalized first-order coherence function $-\text{Im} g^{(1)}$ which dominates at long time-separations.

density n . For an EP system at cryogenic temperatures $T \sim 22$ K, the limit $\theta \gg 1$ is satisfied for time-separations much longer than approximately 350 fs.

B. Measurement of coherence with interferometry: Optical applications

The first-order coherence function is experimentally accessible in the intensity pattern of an interferometer, most commonly of the Michelson or Mach-Zhender type. We consider the case of an optical interferometer, however the basic theory applies to many other types of waves. EP systems well below the BEC transition are approximately unpolarized, and therefore the illuminating source field can be treated as a scalar field u_S . We will assume u_S is stationary and ergodic. For a balanced Michelson interferometer which inverts in the x -direction

and an intensity profile with (at least) x -symmetry, the output intensity is

$$\langle I(\mathbf{r}) \rangle = \frac{1}{2} \langle I_S(\mathbf{r}) \rangle (1 + \mathcal{V}(\mathbf{r}, \tau)) \quad (6)$$

where $I_S = \epsilon_0 c |u_S|^2 / 2$ is the source intensity, ϵ_0 is the permittivity of free-space, c is the speed of light in vacuum, and $\tau = t - t'$ is the time-delay between interferometry arms, set by the path-length difference. The brackets $\langle \cdot \rangle$ denote the time (ensemble) average in the classical (quantum) regime. The dependence on the time-delay τ may be very strong for light with a short coherence time. The visibility function \mathcal{V} is related to the first-order coherence function as

$$\mathcal{V}(\mathbf{r}, \tau) = \frac{\epsilon_0 c}{2 \langle I_S(\mathbf{r}) \rangle} \text{Re} \left\{ G^{(1)}((x, y, z), (-x, y, z), \tau) \right\} \quad (7)$$

from which the traditional visibility V measured from the contrast of interference fringes is derived $V = |\mathcal{V}|$. The visibility satisfies $0 \leq V \leq 1$. In the limit of complete coherence, $V = 1$, the contrast of the interference fringes is maximized, ranging from the maximum intensity to zero intensity. In the limit of complete incoherence (although physically the coherence length is lower-bounded by the light wavelength [24]), $V \approx 0$ and the contrast of the interference fringes is minimized.

Optical fields with partial coherence sit between the two limiting cases, diffracting and interfering differently than their completely incoherent and completely coherent counterparts. The paraxial propagation of completely coherent optical fields in free space can be generalized to the quasi-monochromatic partially coherent case [24–26]. A quasi-monochromatic beam has a small but finite spectral width $\Delta\nu$ and can exhibit interesting spectral anomalies near singular points, points of zero intensity [27–29]. The finite spectral width is a result of a finite coherence time which suggests that the first-order coherence function may depend strongly on the time-delay τ . But so long as the time-delay τ is much smaller than the inverse of the spectral width $1/\Delta\nu$, then its effect can be approximated as a phase factor in the first-order coherence function [25]. We primarily focus on the spatial behavior of the first-order coherence function and assume the time-delay to be optimized $\tau = 0$, unless otherwise stated.

For the remainder of the paper, we will use conventional optics nomenclature. (1) The mutual coherence function Γ refers to the first-order coherence function $G^{(1)}$ of the optical field while the mutual intensity function is the mutual coherence function for zero time-delay $\tau = 0$. (2) The averaged intensity is defined via the mutual intensity function as $I(\mathbf{r}) = \epsilon_0 c \Gamma(\mathbf{r}, \mathbf{r}) / 2$ (similarly to the particle density $n(\mathbf{r}) = G^{(1)}(\mathbf{r}, \mathbf{r})$ in a massive gas). With this definition, we drop the brackets $\langle \cdot \rangle$ as the mutual intensity function is already averaged. The visibility function \mathcal{V} in Eq. 7 can be calculated entirely in terms of the mutual coherence function.

Given a mutual coherence function Γ_0 in the plane $Z = 0$ with coordinates \mathbf{s}_1 and \mathbf{s}_2 , the propagated mutual intensity function in a plane of constant Z with coordi-

ates \mathbf{r}_1 and \mathbf{r}_2 is calculated via an integral transform. In particular, the far-field Fresnel and Fraunhofer approximations [30] yield [25]

$$\Gamma_{\text{Fresnel}}(\mathbf{r}_1, \mathbf{r}_2, Z, \tau) = \frac{1}{\lambda^2 Z^2} e^{i\frac{\bar{k}}{2Z}(r_1^2 - r_2^2)} \mathfrak{F} \left\{ \Gamma_0(\mathbf{s}_1, \mathbf{s}_2, \tau) P(\mathbf{s}_1) P^*(\mathbf{s}_2) e^{i\frac{\bar{k}}{2Z}(s_1^2 - s_2^2)} \right\} \left(\mathbf{f}_1 = \frac{\bar{k}\mathbf{r}_1}{Z}, \mathbf{f}_2 = \frac{\bar{k}\mathbf{r}_2}{Z} \right) \quad (8)$$

$$\Gamma_{\text{Fraunhofer}}(\mathbf{r}_1, \mathbf{r}_2, Z, \tau) = \frac{1}{\lambda^2 Z^2} e^{i\frac{\bar{k}}{2Z}(r_1^2 - r_2^2)} \mathfrak{F} \left\{ \Gamma_0(\mathbf{s}_1, \mathbf{s}_2, \tau) P(\mathbf{s}_1) P^*(\mathbf{s}_2) \right\} \left(\mathbf{f}_1 = \frac{\bar{k}\mathbf{r}_1}{Z}, \mathbf{f}_2 = \frac{\bar{k}\mathbf{r}_2}{Z} \right) \quad (9)$$

where $\mathfrak{F}\{\cdot\}$ is the four-dimensional Fourier transform with respect to the alternating kernel $e^{-i(\mathbf{f}_1 \cdot \mathbf{s}_1 - \mathbf{f}_2 \cdot \mathbf{s}_2)}$, $\bar{\lambda}$ is the mean wavelength of the quasi-monochromatic light, $\bar{k} = 2\pi/\bar{\lambda}$ is the mean wavenumber, and P is the (possibly complex) transmission of the aperture at $Z = 0$.

Various simplifications of this calculation exist. For one, the appearance of a Fourier transform suggests application of the convolution theorem. Additionally, for isotropic correlations which only depends on the magnitude of the separation $|\mathbf{s}_1 - \mathbf{s}_2|$, the intensity can be calculated with Schell's theorem [31, 32]. Numerically, the existence of fast Fourier transform algorithms and parallel computation may aid calculations, as discussed in Ref. [33] for the completely coherent case. However, it should be noted that the completely coherent case only requires a two-dimensional integral rather than a four-dimensional integral.

The difficulty of the propagation is rooted in the functional form of the correlations at $Z = 0$ and the effect of the aperture as modeled by the aperture transmission function P . The intensity of partially coherent light after a physical (finite-sized) circular aperture has been investigated for various functional forms of correlations including Gaussian and Bessel-function [34–36]. Moreover, the mutual intensity function has been investigated for two-slit interference [37, 38]. To the best of our knowledge, propagated Bose gas correlations have not been investigated.

C. Condensate and coherent fraction

Returning to the theory of Bose gases, we recall the definition of the condensate fraction n_0 . Loosely, the condensate fraction is given by the long-range limiting value of the normalized first-order coherence function [39]. More formally, the general expression in d -dimensions is

$$n_0 = \frac{\int d^d r_1 d^d r_2 \phi_0^*(\mathbf{r}_1) G^{(1)}(\mathbf{r}_1, \mathbf{r}_2) \phi_0(\mathbf{r}_2)}{\int d^d r G^{(1)}(\mathbf{r}, \mathbf{r})} \quad (10)$$

where ϕ_0 is the eigenfunction of $G^{(1)}$ with the largest occupation eigenvalue [40]. In the noninteracting case, ϕ_0

is simply the single-particle eigenfunction of the Hamiltonian with the largest occupation, normally the ground-state. With the assumption of homogeneity, ϕ_0 is constant and $G^{(1)}$ only depends on the magnitude of the separation vector $\delta\mathbf{r} = \mathbf{r}_1 - \mathbf{r}_2$ so the expression becomes

$$n_0 = \frac{\int d^d \delta r G^{(1)}(2\delta r)}{\int d^d r G^{(1)}(\mathbf{r}, \mathbf{r})} \quad (11)$$

Motivated by the condensate fraction, we define the coherent fraction of an optical field which is agnostic of the underlying phase (i.e. does not necessarily imply BEC). In particular, we would like it to be measurable in interferometry experiments like those discussed in Sec. II B. Therefore, we define the coherent fraction C of an optical field as

$$C = \frac{|\int d^2 r \text{Re}(\Gamma(\mathbf{r}, -\mathbf{r}, \tau))|}{\int d^2 r \Gamma(\mathbf{r}, \mathbf{r}, 0)} \quad (12)$$

The integrand of the numerator is simply proportional to $I(\mathbf{r}) \mathcal{V}(\mathbf{r}, \tau)$, assuming isotropic correlations. If the mutual intensity function is not isotropic, then the visibility needs to be measured for all orientations of the interferometer, in principle. The coherent fraction is bounded $0 \leq C \leq 1$ and conserved under propagation by Eq. 8 and Eq. 9, see Appendix C 1 for details. While the (normalized) mutual intensity function provides a local measure of coherence, the coherent fraction provides a global measure of coherence for the entire optical field.

The principal difference between the definition of the coherent fraction C and the condensate fraction n_0 is the real part in the numerator. This adjustment ensures that the coherent fraction is directly measurable in interferometry experiments through the contrast of interference fringes, even for nonzero time-delay which generically produce complex-valued correlations. The imaginary part and, hence, magnitude and argument of a complex-valued mutual coherence function can in principle be calculated via Hilbert transform relations [25]. Practically, the integration in Eq. 12 can only be performed over a finite range which produces small corrections to the coherent fraction so long as the mutual coherence function is sufficiently localized. However, the localization condition is generically broken in the case of

an optical field diffracting through a small aperture, as discussed throughout this paper.

III. RESULTS

In this section we present the bulk of our results. First, we calculate the coherent fraction for a free-propagating, partially coherent optical field measured by an ideal interferometer with zero time-delay $\tau = 0$. The results are plotted in Fig. 2. While we find qualitative agreement with experimental measurements from Ref. [19], the results fail to explain two distinct features, (1) a smaller coherent fraction at low densities and (2) a saturation at $C \approx 0.8 < 1$ at high densities, as shown in Fig. 4. To this end, we investigate how diffraction and a finite time-delay between the interferometry arms may affect the coherent fraction. Our analysis suggests that diffraction losses artificially increase the coherent fraction a small amount which, however, can be minimized by optimizing the optical apparatus. In contrast, a finite time-delay can decrease the measured coherent fraction significantly in the low-density regime. Lastly, we note that the buildup of coherence is not formally described by a power-law, although over limited parameter ranges one may approximately hold. For this reason, we do not extract power-law exponents and instead employ the exact theory results.

A. Coherent fraction with no diffraction

As a point of comparison, we begin by calculating the coherent fraction for free-propagating partially coherent optical field. We assume an ideal interferometer with zero time-delay $\tau = 0$ and a mutual intensity function which takes the generic form $\Gamma_0(\mathbf{s}_1, \mathbf{s}_2) = \sqrt{I(\mathbf{s}_1)I(\mathbf{s}_2)}g^{(1)}(|\mathbf{s}_1 - \mathbf{s}_2|)$. Specifically, we first consider a Gaussian-Schell model source [24, 26, 41] so that the mutual intensity in the plane $Z = 0$ with coordinates \mathbf{s}_1 and \mathbf{s}_2 is given by $\Gamma_0(\mathbf{s}_1, \mathbf{s}_2) = |A|^2 e^{-(s_1^2+s_2^2)/\sigma^2} e^{-(s_1-s_2)^2/\xi^2}$ where A is the (complex) amplitude of the scalar field, σ is the width of the Gaussian intensity profile, and ξ is the coherence length. The coherent fraction C_{GS} measured over a disk of radius a is then

$$C_{\text{GS}} = \frac{1}{1 - e^{-2a^2/\sigma^2}} \frac{1}{1 + 2\sigma^2/\xi^2} \left(1 - e^{-2a^2/\sigma^2 - 4a^2/\xi^2}\right) \quad (13)$$

Various limits can be derived. First, removing the aperture $a \rightarrow \infty$ with the width σ and coherence length ξ fixed yields $C_{\text{GS}} = 1/(1 + 2\sigma^2/\xi^2)$ which can be verified with the Fresnel propagation integral Eq. 8. Using the Fraunhofer propagation integral Eq. 9, the coherent fraction is $C_{\text{GS}} = \xi^2/2\sigma^2$. This result matches the asymptotic behavior of Eq. 13 for $\xi \ll \sigma$; the lack of an aperture limits the applicability of the Fraunhofer approximation.

On the other hand, the limit of uniform intensity $\sigma \rightarrow \infty$ with the aperture radius a and coherence length ξ fixed yields $C_{\text{GS}} = \xi^2 (1 - e^{-4a^2/\xi^2})/4a^2$. In contrast to the limit of no aperture, this result can be verified with the Fraunhofer propagation integral Eq. 9. Lastly, the limit of complete coherence $\xi \rightarrow \infty$ with the width σ and aperture radius a fixed yields the expected result $C_{\text{GS}} = 1$.

Second, we calculate the coherent fraction for a source with Bose gas correlations. In contrast to the Gaussian calculation, we fix $\xi = \xi_0$ at the classical value which no longer plays the role of the coherence length, as suggested by Fig. 1, and instead vary the fugacity z . The mutual intensity function in the plane $Z = 0$ with coordinates \mathbf{s}_1 and \mathbf{s}_2 is given by

$$\Gamma_0(\mathbf{s}_1, \mathbf{s}_2) = \frac{|A|^2 e^{-(s_1^2+s_2^2)/\sigma^2}}{-\log(1-z)} \sum_{j=1}^{\infty} \frac{z^j}{j} e^{-(s_1-s_2)^2/j\xi_0^2} \quad (14)$$

where A and σ retain the same meaning. The coherent fraction C_{BG} measured over a disk of radius a is then

$$C_{\text{BG}} = \frac{1}{-\log(1-z)} \sum_{j=1}^{\infty} \frac{z^j}{j} C_{\text{GS}}(\sqrt{j}\xi_0) \quad (15)$$

where $C_{\text{GS}}(\sqrt{j}\xi_0)$ denotes the Gaussian-Schell result Eq. 13 with the adjusted coherence length $\sqrt{j}\xi_0$. The behavior of Eq. 15 is investigated in Appendix B for various limits, and the results are shown in Fig. 2. The coherent fraction after removing the aperture $a \rightarrow \infty$ with the width σ and coherence length ξ fixed is shown in Fig. 2a, and the coherent fraction in the limit of uniform intensity $\sigma \rightarrow \infty$ with the aperture radius a and coherence length ξ fixed is shown in Fig. 2b. While qualitatively similar, the coherent fraction differs significantly for a fixed fugacity z , as shown in Fig. 2c. In particular, the coherent fraction in the limit of no aperture is always higher than the coherent fraction in the limit of uniform intensity since the aperture places a sharp cutoff on the points which can contribute to the coherence. We highlight an approximate expression for the coherent fraction C_{BG} in the case of uniform intensity $\sigma \rightarrow \infty$ with the aperture radius a and classical coherence length ξ_0 fixed

$$C_{\text{BG}} = \frac{1}{-\log(1-z)} \frac{\xi_0^2}{4a^2} \times \left(\frac{z}{1-z} - \frac{4aK_1(4a\sqrt{-\log(z)}/\xi_0)}{\xi_0\sqrt{-\log(z)}} \right) \quad (16)$$

where K_ν is the ν -order modified Bessel function of the second kind. This expression is accurate in the limit $z \rightarrow 1$ which is experimentally important. The limiting behavior of Eq. 16 (for fugacities z even closer to 1) is presented in Eq. B10.

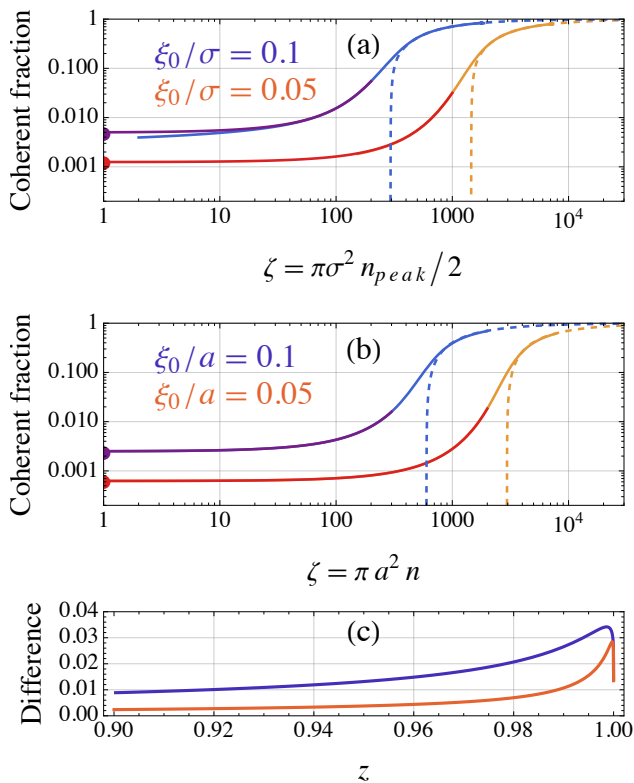


FIG. 2. Ideal coherent fraction for a Gaussian beam with Bose gas correlations incident on a circular aperture as a function of particle number ζ . (a) Coherent fraction for a Gaussian beam of width σ in the limit of no aperture (see text) as a function of the particle number $\zeta = \pi\sigma^2 n_{\text{peak}}/2$ measured in terms of the peak density n_{peak} . Two values of the classical coherence length relative to the beam width are shown, $\xi_0/\sigma = 0.1$ (blue-purple) and 0.05 (orange-red). For different regimes of particle number, different expressions for the coherent fraction are used: Coherent fraction from series expansion in the fugacity Eq. 15 (solid purple or red), coherent fraction from Euler-Maclaurin formula (solid blue or orange), and asymptotic behavior (dashed blue or orange), see Appendix B for details. (b) Coherent fraction for a beam incident on an aperture of radius a in the limit of uniform intensity (see text) as a function of the particle number $\zeta = \pi a^2 n$ measured in terms of the homogeneous density n . Expressions for the coherent fraction derived identically to those in (a) are used in (b), see Eq. 15, Eq. 16, and Appendix B for details. (c) Comparison of the coherent fractions from the limiting cases in (a) and (b). The difference is given by (a) - (b).

B. Diffraction of a partially coherent source with Bose gas correlations

In deriving Eq. 13 and 15, we assume that we can simply integrate over a disk of radius a . However, this disk is physically implemented as a circular aperture in the imaging system. While previous discussion in Sec. II C and Appendix C explain that the precise diffraction pattern is not needed to calculate the coherent fraction, we model the diffraction of the partially coherent source in

order to gain insight into the nature of the experimental signal and investigate diffraction losses.

We define the (real) transmission function of the aperture as the indicator function of the aperture

$$P(\mathbf{s}) = \Theta(a - s) = \begin{cases} 1 & s \leq a \\ 0 & s > a \end{cases} \quad (17)$$

where Θ is the Heaviside step-function and a is the aperture radius. If a is sufficiently small relative to the beam width of the incident optical field, then the field can be approximated as having a uniform intensity over the aperture, i.e. taking the limit $\sigma/a \rightarrow \infty$. Propagating the initial mutual intensity function ($\tau = 0$) in the Fraunhofer limit with Eq. 9, we obtain the mutual intensity function of the diffracted light in the far-field from which we can extract the intensity and visibility function. The simplified propagation integrals are presented in Appendix D.

In Fig. 3a and b, we plot the intensity (a) and visibility function (b) for Gaussian correlations. The visibility function is always unity on axis; this result is obvious from the definition of the visibility but can be thought of as a specific case of the general result presented in Ref. [37] which states that equidistant points in Young's double slit experiment exhibit complete coherence regardless of the state of coherence of the illuminating light. Generically, the visibility exhibits oscillations and phase singularities, which are known to occur in Young's double slit experiment [42].

The oscillation amplitude dips after the central peak, before recovering to unity as the distance from the axis increases. This trend is particularly evident in Fig. 3b for $\xi/a = 0.5$ and 1. Additionally, there are points which exhibit complete incoherence $V = 0$ regardless of the initial state of coherence of the optical field (so long as it is not completely coherent). We stress that these oscillations are physically distinct from the fringes observed in interferometry experiments; while fringes arise from the geometry of the interferometer (careful misalignment of interfering beams), the oscillations in the visibility are a result of the partial coherence of the illuminating source. In experiment, this suggests amplitude modulation of fringes. However, if measurements take place in the very far-field $Z \gg akr$ and the intensity becomes too low away from the axis, then only the near-axis region is considered.

A similar optical analysis can be performed for Bose gas correlations. The intensity is plotted in Fig. 3c while the visibility function is plotted in Fig. 3d, exhibiting similar oscillations. A qualitative difference, however, is that the strength of the anti-correlations (negative values) is much weaker. In contrast, Fig. 3b shows oscillations between correlations and anti-correlations which are roughly equal in magnitude.

In Ref. [19], the diffraction pattern is focused by a lens which imposes a second circular aperture on the signal. The coherent fraction is then measured in the focal plane where the optical field is the Fourier transform of the source, assuming an infinite lens pupil. Relaxing this

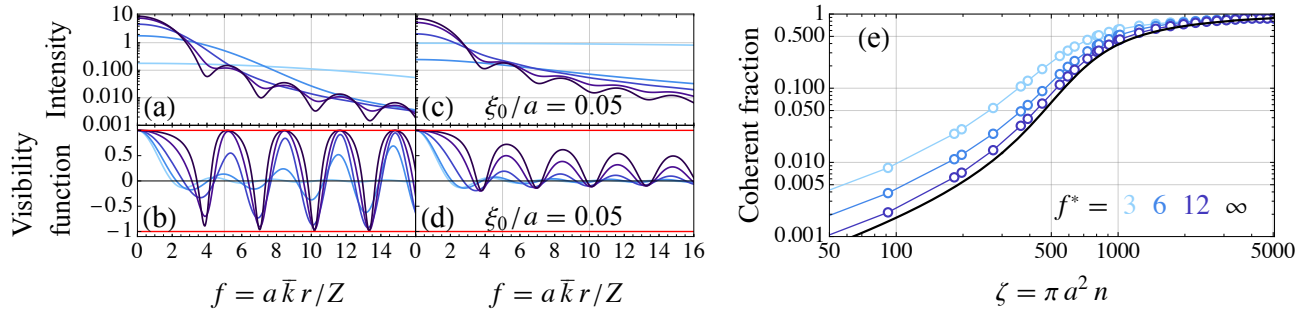


FIG. 3. Analysis of a homogeneous, partially coherent source diffracted by a circular aperture. (a) Intensity of a source with Gaussian correlations in units of $(\epsilon_0 c/2) (|A|^2 a^4/\lambda^2 Z^2)$ for various coherence lengths relative to the aperture radius $\xi/a = 0.14, 0.5, 1, 2,$ and 3.5 (lighter blue for smaller ξ/a and darker blue for larger ξ/a). (b) Visibility function for the same source and coherence lengths as (a) showing oscillations between regions of correlation and anti-correlation. The visibility function is bounded by ± 1 (solid red). (c) Intensity of a source with Bose gas correlations in units of $(\epsilon_0 c/2) (|A|^2 a^4/\lambda^2 Z^2)$ for various particle numbers in the aperture $\zeta = \pi a^2 n = 10, 1540, 3185, 5890,$ and 11125 (lighter blue for smaller ζ and darker blue for larger ζ), equivalently treated as fugacities $z = 1 - \exp(-\xi_0^2 \zeta/a^2)$ with the classical coherence length relative to the aperture radius $\xi_0/a = 0.05$ fixed. (d) Visibility function for the same source and particles numbers in the aperture as (c) showing oscillations between regions of correlation and weak anti-correlation. The visibility function is bounded by ± 1 (solid red). (e) Coherent fraction of a source with Bose gas correlations with diffraction losses (solid blue and markers) calculated from the intensity and visibility function in (c) and (d), respectively. Integration is performed to $f^* = a\bar{k}r^*/Z$ where r^* is the position in the imaging plane, and the coherent fraction for $\zeta > 0$ is taken relative to the zero density $\zeta = 0$ limit which corresponds to the classical Gaussian result. The results with diffraction losses converge to the exact coherent fraction (solid black) in the limit $f^* \rightarrow \infty$.

assumption by introducing a finite lens radius, but ensuring it is large enough to limit significant diffraction effects (i.e. that integration in the focal plane can be effectively performed over the entire optical signal), we study the corrections to the coherent fraction by numerically integrating the intensities and visibility functions from Fig. 3c-d. The result is shown in Fig. 3e for various integration limits. A partial analytic analysis is presented in Appendix C 2. In general, a smaller integration window increases the measured coherent fraction since the mutual intensity decays more quickly than the intensity.

C. Corrections to the coherent fraction due to finite time-delay

The natural time-scale of the noninteracting, equilibrium Bose gas is the thermal time $\hbar/k_B T$ as introduced in Eq. 5. In the EP system, this should be compared to the inverse spectral width $1/\Delta\nu$ of the monitored quasi-monochromatic optical field. At cryogenic temperatures $T \sim 22$ K, the thermal time is approximately 350 fs while the coherence time in the classical Maxwell-Boltzmann limit is $\pi\hbar/k_B T$ or approximately 1 ps (see Appendix E). This is comparable to the inverse spectral width on the order of 1 ps observed in experiment in the low-density limit [19]. Notably, the optical signal from EP systems is known to exhibit spectral inhomogeneous broadening in the high-density regime [2]. Due to the limited time-resolution, we expect there to be a small but finite time-delay in interferometry experiments.

A finite time-separation generically reduces the

strength of the equal-position correlations, as is clear from Fig. 1b. However, the correlations of far-separated positions can actually become stronger at finite time-separations as the wavefunction evolves and propagates. This behavior combined with the real-part in the definition Eq. 12 has counterintuitive implications on global measurements of coherence, for example leading to non-monotonic and oscillatory behavior of the coherent fraction with increasing (classical) coherence length, or equivalently decreasing temperature, and increasing time-separation, see Appendix E for details. The correlation area, on the other hand, is more well-behaved. We include a finite time-delay into the expression for the coherent fraction Eq. 15 by replacing the Gaussian-Schell coherent fraction from Eq. 13 with Eq. E2 to obtain Eq. E5. The modified coherent fraction is shown in Fig. 4 for a small range of time-delays τ between interferometry arms, see Sec. IV for further discussion.

IV. DISCUSSION

Our analysis considers an equilibrium gas of noninteracting EPs in a homogeneous potential landscape. In this section, we discuss the validity of these assumptions and compare to recent experimental results [19].

First, we neglect nonequilibrium effects. Our analysis presumes an equilibrated thermal state rather than a non-equilibrium steady-state. Measurements of the thermal distribution function in Ref. [19] show good agreement with the Bose-Einstein distribution suggesting equilibrium conditions. However, the long-wavelength dy-

namics of EP systems in one and two dimensions are ultimately governed by the KPZ equation [17]. While signatures of KPZ physics have been observed in one dimension [18], the presence of vortices and the algebraically-ordered BKT phase in two dimensions (in equilibrium) makes the experimental detection of KPZ physics more difficult. The analysis in Ref. [43] compares the length-scale for (bare) vortex unbinding, driving the transition to disorder in the BKT regime, to the length-scale for a “rough phase” characteristic of KPZ physics. Generically, the length-scale at which KPZ correlations dominate is much longer than that for BKT correlations. And for finite-sized EP systems, even BKT correlations may be difficult to observe leading to the phenomena of quasi-condensation: effective though not exactly uniform phase and constant long-range correlations across the sample. A finite beam width or the use of an aperture further limits the sensitivity to BKT and KPZ correlations by imposing a limit on the separations probed by coherence measurements.

Second, we neglect interaction effects. Two-body interactions of EP are generically considered to be weak, yet they can still play a crucial role in the system’s correlations and phase, for example facilitating the BKT phase transition. In the dilute limit, the physical two-body interaction is usually replaced by a scalar pseudo-potential contact-interaction with coupling strength g . The coupling strength g induces an interaction length-scale b which is simply proportional to g in three dimensions. Scattering in two dimensions is more complicated, however, which obscures the relation between g and b [44–46]. To estimate the length-scale of perturbations induced by the interaction as observed in the mutual intensity function after the aperture, we compute the interaction energy gn relate it to a momenta $k_g = \sqrt{2mgn}/\hbar^2$ then extract the length-scale $b = Zk_g/k$ motivated by the far-field position variable from Eq. 9. From the values of g , n , and \bar{k} provided in Ref. [19] we find the ratio $k_g/\bar{k} \approx 0.04 \sim 10^{-2}$. However, we note that the measurement of g in EP systems is difficult, and g is often treated as a free parameter. Since this ratio is small, we expect that the interactions do not dramatically alter the first-order coherence function, and that it may be sufficient to approximate the gas as noninteracting away from the critical density.

Additionally, excitonic disorder, modeled as a distribution of excitonic energies and coupling strengths [47], can be effectively described by a modified two-body interaction strength in the low-density regime [48]. For standard EP systems, the modified interaction strength is significantly enhanced in comparison to the disorder-free interaction strength. The effect of excitonic disorder is captured implicitly in the measurement of g .

Lastly, the EP interaction strength is coupled to the disorder in the potential landscape, distinct from excitonic disorder, through the EP density. Potential corrugations introduce another length-scale into the problem, the correlation length of the potential, over which the

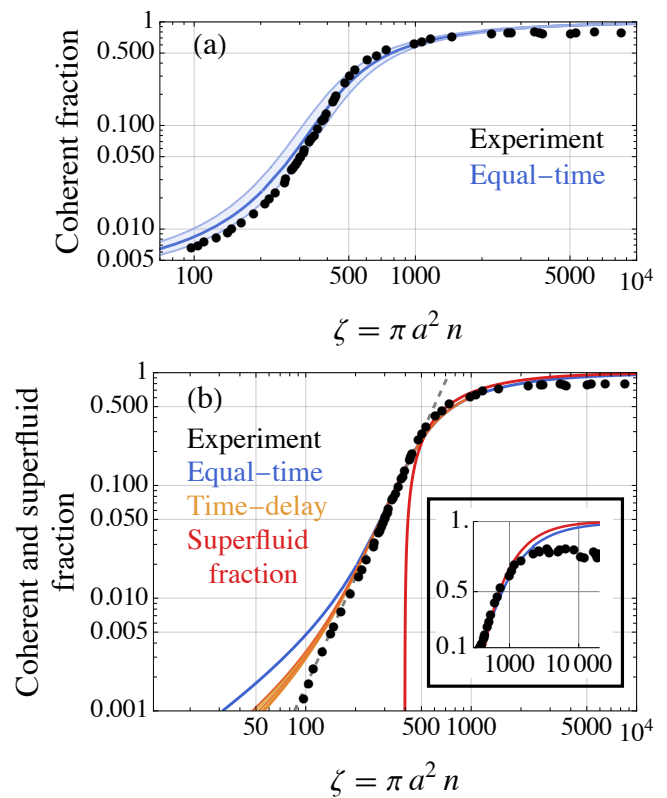


FIG. 4. Comparison of the noninteracting, equilibrium theory presented in the main text to recent experimental results from Ref. [19]. (a) Bare comparison without subtraction of the coherent fraction in the zero-density limit. The experimental coherent fraction measurements (black circles) are plotted in terms of the EP number in the aperture $\zeta = \pi a^2 n$. The theory prediction for the coherent fraction measured by an ideal interferometer with zero time-delay $\tau = 0$ (solid dark blue) is plotted for a range of temperatures $20 \leq T \leq 24$ K with $T = 22$ K the center, consistent with temperature measurements from Ref. [19]. (b) Comparison with subtraction of the coherent fraction in the zero-density limit and power-law behavior. The experimental coherent fraction measurements (black circles) are plotted in terms of the EP number in the aperture $\zeta = \pi a^2 n$ with the observed $\zeta^{3.2}$ power-law (dashed gray) as a guide. The theory prediction for the coherent fraction measured by an ideal interferometer with zero time-delay $\tau = 0$ (solid blue) is plotted along with the coherent fraction measured by an interferometer with finite time-delay $13 \leq \tau \leq 15$ ps (multiple solid orange), all at temperature $T = 22$ K. The superfluid fraction (solid red) defined in Eq. 18, which only exists for finite interactions, matches the near-transition data. We use $g = 2.11 \mu\text{m}^2$ from Ref. [19] which yields $\gamma = 6.68 \times 10^{-6}$ for the dimensionless interaction strength (see text). (Inset) The experimental coherent fraction measurements deviate significantly from the theory curves at high densities, possibly a result of systematic uncertainties associated with fringe measurement in the experimental interferometer. All theory curves assume an aperture radius of $a = 6 \mu\text{m}$.

magnitude of the first-order coherence varies [2]. In the low-density regime, we assume that chemical potential is large enough compared to the variations of the potential landscape so that the EP sample is approximately homogeneous. For high densities, this assumption is expected to fail.

With these notes in mind, we compare the predictions of the finite-sized, noninteracting, equilibrium theory to the recent experimental results from Ref. [19] in Fig. 4. The model for an ideal interferometer with zero time-delay $\tau = 0$ has no free parameters; the inputs are only the EP mass $m = 1.515 \times 10^{-4} m_e$, where $m_e = 9.109 \times 10^{-31}$ kg is the electron mass, the temperature $T = 22$ K entering through the classical coherence length $\xi_0 = \lambda_T / \sqrt{\pi}$, and the aperture radius $a = 6 \mu\text{m}$. However, experimental measurements of the temperature show significant fluctuations, and, therefore, we include theory curves for a range of temperatures $20 \leq T \leq 24$ K in Fig. 4a which bound the experimental data.

As a comparison to the zero time-delay results, we also show results for a small range of time-delays around $\tau = 14$ ps in Fig. 4b yielding slightly improved agreement in the low-density regime. The experimental time-delay can be estimated from the uncertainty of the path-length difference $\delta\ell$ between the interferometry arms as $\tau \sim \delta\ell/c$. However, the finite coherence time in the zero-density limit can effect the measurement of $\tau = 0$ by broadening the (time) visibility signal. While we assume the time-delay to be approximately on the order of $\delta\ell/c$ (which is also on the order of the lowest coherence time measured in Ref. [19]), we otherwise treat it as a free parameter in order to explore its effect on the theory. The coherent fraction in the zero-density limit Eq. E2 is relatively insensitive to small but finite time-delays as the exponential term dominates when $\theta < 1/\xi_0$. However, as the time-delay increases, the expression is notably non-monotonic. At long times there is an exponential decay of the coherent fraction to zero. For Fig. 4b, we select a small time-delay $\tau = 14$ ps which decreases the baseline coherent fraction. The result for finite time-delay becomes coincident with the $\tau = 0$ result at high densities.

While the condensate and coherent fraction can be defined for noninteracting gases, the superfluid fraction only exists for interacting gases. In terms of the parameters used in this paper, we calculate the superfluid fraction s assuming an infinite system as [46, 49]

$$s = 1 - \frac{1}{\zeta \xi_0^2 / a^2} \int_0^\infty dx \left(1 - \frac{1}{\sqrt{1 + \frac{x^2}{\gamma^2 \zeta^2 \xi_0^4 / a^4}}} \right) \frac{x e^x}{(e^x - 1)^2} \quad (18)$$

where γ is a dimensionless parameter which characterizes the interaction strength, microscopically given by $\gamma = mg/2\pi\hbar^2$. We have brought the integral into a dimensionless form with the change of variables $x = \beta\epsilon_{\text{Bog}}(k)$ where $\epsilon_{\text{Bog}}^2(k) = gmk^2/m + k^4/4m^2$ is the usual Bogoliubov excitation spectrum. The superfluid fraction

is compared to the coherent fraction in Fig. 4 showing decent agreement near the transition. However, as with the noninteracting theory, there is still a disagreement in the high-density regime past the transition, possibly a result of systematic uncertainties associated with fringe measurement in the experimental interferometer.

V. CONCLUSION

The results presented in this paper are broadly applicable to experiments with partially coherent light; in particular, they may be helpful in measurements of coherence in finite-sized EP systems characterized by Gaussian or more general Bose gas correlations. We have analyzed the behavior of the coherent fraction with various system parameters including the particle number via analytic and numerical methods and discussed how the intensity and visibility function are altered by the presence of an aperture. Our results provide a baseline, without fit parameters, to which interacting models and experimental data can be compared. In particular, we find good agreement to the data of Ref. [19] over nearly three orders of magnitude in the coherence fraction and a factor of approximately 50 in the EP number.

ACKNOWLEDGMENTS

This research is funded in part by the Gordon and Betty Moore Foundation through grant GBMF12763 to Peter Littlewood, who thanks Shuolong Yang for discussions. The experimental work at Pittsburgh and sample fabrication at Princeton were supported by the National Science Foundation through grant DMR-2306977.

Appendix A: Asymptotic behavior of Bose gas correlations

The long-range behavior of the first-order coherence function is determined by the low-momentum behavior of the Bose-Einstein distribution [50, 51]. Expansion of the exponential in powers of k_{\parallel} yields

$$\tilde{n}(\mathbf{k}_{\parallel}) = \frac{z}{e^{\beta k_{\parallel}^2 / 2m} - z} = \frac{z}{1 + \beta k_{\parallel}^2 / 2m + \mathcal{O}(k_{\parallel}^4)} - z \quad (A1)$$

After inverse Fourier transform of the rational function, we obtain the asymptotic form of the first-order coherence function

$$G^{(1)}(\mathbf{r}, \mathbf{r}') \sim \frac{2z}{\lambda_T^2} K_0 \left(\frac{2\sqrt{\pi}\sqrt{1-z}|\mathbf{r} - \mathbf{r}'|}{\lambda_T} \right) \quad (A2)$$

where K_ν is the ν -order modified Bessel function of the second kind. Since this result works best in the limit $z \rightarrow 1$, it is also common to expand the fugacity $z =$

$1 + \beta\mu + \mathcal{O}(\mu^2)$ in terms of the chemical potential in the limit $\mu \rightarrow 0^-$.

Finally, we can estimate the fugacity z at which the Bose gas correlations become dominant. The length-scale ℓ associated with the asymptotic first-order coherence function is

$$\ell = \frac{\lambda_T}{2\sqrt{\pi}\sqrt{1-z}} \sim \frac{1}{\sqrt{-2m\mu}} \quad (\text{A3})$$

and, therefore, the length ℓ surpasses the classical coherence length $\lambda_T/\sqrt{\pi}$ at $z = 3/4$.

Appendix B: Behavior of the free-propagating coherent fraction

The behavior of Eq. 15 for small fugacities $z \ll 1$ is easy to obtain since only a few terms in the sum are necessary. For larger fugacities, in particular in the limit $z \rightarrow 1$, the calculation becomes cumbersome, and it is helpful to make an integral approximation. In this section of the appendix, the behavior of the coherent fraction at finite fugacity in the limit of no aperture and in the limit of uniform intensity is investigated.

1. Limit of no aperture

We start from the coherent fraction in Eq. 15 and obtain

$$C_{\text{BG}} = \frac{1}{-\log(1-z)} \sum_{j=1}^{\infty} \frac{z^j}{j + 2\sigma^2/\xi_0^2} \quad (\text{B1})$$

in the limit of no aperture $a \rightarrow \infty$ with the width σ and the classical coherent length ξ_0 fixed. Using the Euler-Maclaurin formula, which works well for $z \rightarrow 1$, we make the approximation

$$C_{\text{BG}} \approx \frac{1}{-\log(1-z)} \left(\int_1^{\infty} dj \frac{z^j}{j + 2\sigma^2/\xi_0^2} + \frac{z}{2 + 4\sigma^2/\xi_0^2} \right) \quad (\text{B2})$$

$$\approx \frac{1}{-\log(1-z)} \left(\frac{-\text{li} \left(z^{1+2\sigma^2/\xi_0^2} \right)}{z^{2\sigma^2/\xi_0^2}} + \frac{z}{2 + 4\sigma^2/\xi_0^2} \right) \quad (\text{B3})$$

where li is the logarithmic integral. Finally, we expand about $z = 1$ to obtain the limiting behavior

$$C_{\text{BG}} \sim \frac{1}{z^{2\sigma^2/\xi_0^2}} \left(1 - \frac{\log(1 + 2\sigma^2/\xi_0^2) + \gamma}{-\log(1-z)} \right) \quad (\text{B4})$$

where γ is the Euler-Mascheroni constant. This expression is accurate to the order 10^{-3} .

We can also investigate the behavior of the coherent fraction C_{BG} with the width σ and the classical coherence length ξ_0 at small but finite fugacity $0 < z \ll 1$ via a series expansion. First, in the limit $\xi_0 \gg \sigma$ we find

$$C_{\text{BG}} = \frac{1}{-\log(1-z)} \sum_{j=0}^{\infty} (-1)^j 2^j \left(\frac{\sigma}{\xi_0} \right)^{2j} \text{Li}_{j+1}(z) \quad (\text{B5})$$

where Li_j is the polylogarithm of order j . The leading-order term $j = 0$ ensures that $C_{\text{BG}} = 1$ in the limit $\xi_0 \rightarrow \infty$ with σ fixed since $\text{Li}_1(z) = -\log(1-z)$. Similarly, in the limit $\xi_0 \ll \sigma$ we find

$$C_{\text{BG}} = \frac{1}{-\log(1-z)} \frac{1}{2} \left(\frac{\xi_0}{\sigma} \right)^2 \sum_{j=0}^{\infty} \frac{(-1)^j}{2^j} \left(\frac{\xi_0}{\sigma} \right)^{2j} \text{Li}_{-j}(z) \quad (\text{B6})$$

The leading-order term $j = 0$ yields quadratic scaling which matches the Gaussian-Schell result C_{GS} in the limit $z \rightarrow 0$.

2. Limit of uniform intensity

We start from the coherent fraction in Eq. 15 and obtain

$$C_{\text{BG}} = \frac{1}{-\log(1-z)} \frac{\xi_0^2}{4a^2} \sum_{j=1}^{\infty} z^j \left(1 - e^{-4a^2/j\xi_0^2} \right) \quad (\text{B7})$$

in the limit of uniform intensity $\sigma \rightarrow \infty$ with the aperture radius a and the classical coherence length ξ_0 fixed. We can evaluate the series in two parts. The first is a geometric series. For the second part, we use the Euler-Maclaurin formula which works well in the limit $z \rightarrow 1$

$$C_{\text{BG}} \approx \frac{1}{-\log(1-z)} \frac{z}{1-z} \frac{\xi_0^2}{4a^2} - \frac{1}{-\log(1-z)} \frac{\xi_0^2}{4a^2} \int_1^{\infty} dj z^j e^{-4a^2/j\xi_0^2} - \frac{z}{-\log(1-z)} \frac{\xi_0^2}{8a^2} e^{-4a^2/\xi_0^2} \quad (\text{B8})$$

To evaluate the integral, we extend the lower integration bound from 1 to 0 since the integrand is negligible for $j \ll 4a^2/\xi_0^2$ and usually $4a^2/\xi_0^2 \gg 1$ for experimental systems. Then

$$\int_0^{\infty} dj z^j e^{-4a^2/j\xi_0^2} = \frac{4aK_1 \left(4a\sqrt{-\log(z)}/\xi_0 \right)}{\xi_0 \sqrt{-\log(z)}} \quad (\text{B9})$$

where K_1 is the first-order modified Bessel function of the second kind. In turn, we also neglect the boundary term from the Euler-Maclaurin formula. Finally, we expand about $z = 1$ to obtain the limiting behavior

$$C_{\text{BG}} \sim 1 - \frac{2 \log(2a/\xi_0)}{-\log(1-z)} \quad (\text{B10})$$

which is accurate to the order of 10^{-3} .

We can also investigate the behavior of the coherent fraction C_{BG} with the aperture radius a and the classical coherent length ξ_0 at small but finite fugacity $0 < z \ll 1$ via a series expansion. First, in the limit $\xi_0 \gg a$ we expand the exponential in a power series and simplify the sum to obtain

$$C_{\text{BG}} = \frac{1}{-\log(1-z)} \sum_{j=0}^{\infty} \frac{(-1)^j}{(j+1)!} \left(\frac{2a}{\xi_0}\right)^{2j} \text{Li}_{j+1}(z) \quad (\text{B11})$$

The leading-order term $j = 1$ ensures that $C_{\text{BG}} = 1$ in the limit $\xi_0 \rightarrow \infty$ with a fixed since $\text{Li}_1(z) = -\log(1-z)$. Second, in the limit $\xi_0 \ll a$, we ignore the exponential term $e^{-4a^2/j\xi_0^2}$ with the assumption that the fugacity is sufficiently small such that z^j suppresses the exponential term once the summation index j is on the order $j \sim \xi_0^2/4a^2$. Then

$$C_{\text{BG}} \approx \frac{1}{-\log(1-z)} \frac{z}{1-z} \frac{\xi_0^2}{4a^2} \quad (\text{B12})$$

The limiting value for $z \rightarrow 0$ matches the limiting value of the Gaussian-Schell result C_{GS} .

Appendix C: Propagation of the coherent fraction

1. Conservation of the coherent fraction under propagation

The definition of the coherent fraction presented in Eq. 12 is conserved under Fresnel and Fraunhofer prop-

agation. This result is derived as follows. Consider a mutual intensity function of the generic form

$$\Gamma_0(\mathbf{s}_1, \mathbf{s}_2) = \sqrt{I(\mathbf{s}_1)I(\mathbf{s}_2)}g^{(1)}(|\mathbf{s}_1 - \mathbf{s}_2|) \quad (\text{C1})$$

where I is the beam intensity and $g^{(1)}$ is the normalized mutual intensity function (normalized first-order coherence function) defined in the main text. We assume isotropic correlations which only depend on the magnitude of the separation vector $|\mathbf{s}_1 - \mathbf{s}_2|$. The coherent fraction is then

$$C = \frac{\left| \int d^2s \sqrt{I(\mathbf{s})I(-\mathbf{s})} \text{Re}(g^{(1)}(2s)) \right|}{\int d^2s I(\mathbf{s})} \quad (\text{C2})$$

Now we introduce an aperture in the plane $Z = 0$ described by a transmission function P and propagate the mutual intensity function with Eq. 8 to a plane of constant Z with coordinates \mathbf{r}_1 and \mathbf{r}_2 , with Eq. 9 being a limiting case. Applying Eq. 12 we find

$$C = \frac{\left| \text{Re} \int d^2s_1 d^2s_2 \sqrt{I(\mathbf{s}_1)I(\mathbf{s}_2)}g^{(1)}(|\mathbf{s}_1 - \mathbf{s}_2|) P(\mathbf{s}_1) P^*(\mathbf{s}_1) e^{i\frac{k}{2Z}(s_1^2 - s_2^2)} \int_W d^2r e^{-i\frac{k}{Z}\mathbf{r}\cdot(\mathbf{s}_1 + \mathbf{s}_2)} \right|}{\int d^2s_1 d^2s_2 \sqrt{I(\mathbf{s}_1)I(\mathbf{s}_2)}g^{(1)}(|\mathbf{s}_1 - \mathbf{s}_2|) P(\mathbf{s}_1) P^*(\mathbf{s}_1) e^{i\frac{k}{2Z}(s_1^2 - s_2^2)} \int_W d^2r e^{-i\frac{k}{Z}\mathbf{r}\cdot(\mathbf{s}_1 - \mathbf{s}_2)}} \quad (\text{C3})$$

where W is the window in the plane of constant Z over which the coherent fraction is measured. For $W = \mathbb{R}^2$ we obtain Eq. C2 (assuming integration only over the aperture) since the integrals over \mathbf{r} yield Dirac δ -functions. Therefore, the coherent fraction is conserved for all Z .

We note that an alternate definition of the coherent fraction with $|\text{Re}(\Gamma(\mathbf{r}, -\mathbf{r}, \tau))|$ in the numerator integrand of Eq. 12 could be used. This definition gives the ratio of the power of the optical field producing interference fringes to the total power. However, this definition is not, in general, conserved under propagation, although it is lower-bounded by the coherent fraction in the plane $Z = 0$.

2. Correction to coherent fraction due to diffraction losses

In Ref. [19], the optical signal from the EP propagates through an aperture and then a thin lens with the coherent fraction measurement made in the Fourier plane. The propagation of a mutual coherence function Γ_0 through this imaging system is obtained using the Fresnel propa-

gation integral Eq. 8

$$\begin{aligned} \Gamma(\mathbf{q}_1, \mathbf{q}_2) = & \frac{1}{\lambda^4 F^2 Z^2} e^{i\frac{k}{2F}(q_1^2 - q_2^2)} \left\{ \int d^2 s_1 d^2 s_2 d^2 r_1 d^2 r_2 \right. \\ & \cdots \sqrt{I(\mathbf{s}_1) I(\mathbf{s}_2)} g^{(1)}(|\mathbf{s}_1 - \mathbf{s}_2|) P(\mathbf{s}_1) P^*(\mathbf{s}_2) \\ & \cdots e^{i\frac{k}{2Z}(s_1^2 - s_2^2)} P_\ell(\mathbf{r}_1) P_\ell^*(\mathbf{r}_2) e^{i\frac{k}{2Z}(r_1^2 - r_2^2)} \\ & \left. \cdots e^{-i\frac{k}{2}(\mathbf{r}_1 \cdot \mathbf{s}_1 - \mathbf{r}_2 \cdot \mathbf{s}_2)} e^{-i\frac{k}{F}(\mathbf{q}_1 \cdot \mathbf{r}_1 - \mathbf{q}_2 \cdot \mathbf{r}_2)} \right\} \end{aligned} \quad (\text{C4})$$

where F is the focal length of the thin lens, P_ℓ is the pupil function of the thin lens, \mathbf{q}_1 and \mathbf{q}_2 are the position variables in the Fourier plane, position $Z + F$, \mathbf{r}_1 and \mathbf{r}_2 are the position variables at the thin lens, position Z , and finally \mathbf{s}_1 and \mathbf{s}_2 are the position variables in the aperture, position 0, as defined in the previous section. If we assume no pupil function for the thin lens (i.e. an infinite thin lens), then we can perform the integrals of \mathbf{r}_1 and \mathbf{r}_2 to get

$$\begin{aligned} \Gamma(\mathbf{q}_1, \mathbf{q}_2) = & \frac{1}{\lambda^2 F^2} e^{i\frac{k}{2F}(1 - \frac{Z}{F})(q_1^2 - q_2^2)} \left\{ \int d^2 s_1 d^2 s_2 \right. \\ & \cdots \sqrt{I(\mathbf{s}_1) I(\mathbf{s}_2)} g^{(1)}(|\mathbf{s}_1 - \mathbf{s}_2|) P(\mathbf{s}_1) P^*(\mathbf{s}_2) \\ & \left. \cdots e^{-i\frac{k}{F}(\mathbf{q}_1 \cdot \mathbf{s}_1 - \mathbf{q}_2 \cdot \mathbf{s}_2)} \right\} \end{aligned} \quad (\text{C5})$$

which is the standard result that a thin lens performs a Fourier transform of the incoming field by moving the focus at infinity to the focal plane. In this case, the coherent fraction is conserved, as shown in the previous section.

In experiment, however, the lens has a finite size which results in a partial loss of optical signal diffracted from the aperture and vignetting. Assuming that the lens is circular with a radius a_ℓ and neglecting finite size corrections due to the integration over the positions \mathbf{q}_1 and \mathbf{q}_2 in the Fourier plane, we can obtain corrections to the coherent fraction using Eq. C3 with W being the disk of radius a_ℓ . In this case,

$$\int_W d^2 r e^{-i\frac{k}{2}\mathbf{r} \cdot (\mathbf{s}_1 \pm \mathbf{s}_2)} = 2\pi a_\ell^2 \frac{J_1(\bar{k}a_\ell |\mathbf{s}_1 \pm \mathbf{s}_2|/Z)}{\bar{k}a_\ell |\mathbf{s}_1 \pm \mathbf{s}_2|/Z} \quad (\text{C6})$$

where J_ν is the ν -order Bessel function of the first kind. This result can be analyzed in the limit of an infinite lens $\bar{k}a_\ell \rightarrow \infty$ by expressing the first-order Bessel function as an integral

$$J_1\left(\frac{\bar{k}a_\ell |\mathbf{s}_1 \pm \mathbf{s}_2|}{Z}\right) = \frac{|\mathbf{s}_1 \pm \mathbf{s}_2|}{\bar{k}a_\ell Z} \int_0^{\bar{k}a_\ell} dx x J_0\left(\frac{|\mathbf{s}_1 \pm \mathbf{s}_2|}{Z} x\right) \quad (\text{C7})$$

and noting the Bessel function definition of the Dirac delta function

$$\delta(y) = y \int_0^\infty dx x J_0(yx) \quad (\text{C8})$$

Appendix D: Propagation integrals

In this section, we discuss in detail the propagation of an initial mutual intensity function past a circular aperture with transmission function Eq. 17 (without directly calculating the coherent fraction as in Appendix C). We will assume the Fraunhofer limit and use Eq. 9.

First, consider the case Gaussian correlations. The mutual intensity function in the plane $Z = 0$ with coordinates \mathbf{s}_1 and \mathbf{s}_2 is given by $\Gamma_0(\mathbf{s}_1, \mathbf{s}_2) = |A|^2 e^{-(\mathbf{s}_1 - \mathbf{s}_2)^2/\xi^2}$ where A is the (complex) amplitude of the scalar field and ξ is the coherence length. The four-dimensional propagation integral for the mutual intensity function in the Fraunhofer limit Eq. 9 is reduced to a one dimensional integral in the case of the intensity and a two dimensional integral in the case of the mutual intensity function evaluated at the points $\mathbf{r}_1 = -\mathbf{r}_2 = \mathbf{r}$. We list the simplified propagation integrals here.

The intensity is

$$\begin{aligned} I(\mathbf{f}) = & \frac{\epsilon_0 c 2\pi^{3/2} |A|^2 a^4}{2 \lambda^2 Z^2} \\ & \times \int_0^2 d\rho \rho e^{-\rho^2/\xi_r^2} G_{02}^{02}\left(\frac{1/2}{-1} \left| \begin{array}{c} 1 \\ 0 \end{array} \right| \frac{4}{\rho^2}\right) J_0(f\rho) \end{aligned} \quad (\text{D1})$$

where G is the Meijer G -function, J_ν is the ν -order Bessel function of the first kind, $\xi_r = \xi/a$ is the coherence length relative to the aperture radius, and $\mathbf{f} = a\bar{k}\mathbf{r}/Z$ is the dimensionless far-field position with magnitude f . This expression is derived by applying Schell's theorem [31, 32]. There does exist an exact series expansion for the intensity [52], however the integral expression was numerically faster and more accurate in our studies.

The mutual intensity function is derived from the convolution theorem. The general result of applying the convolution theorem to Eq. 9 and changing variables is

$$\begin{aligned} \Gamma(\bar{\mathbf{f}}, \delta\mathbf{f}) = & \frac{|A|^2 a^2}{\lambda^2 Z^2 n} e^{i\frac{Z}{k}\bar{\mathbf{f}} \cdot \delta\mathbf{f}} \int d^2 \bar{\mathbf{g}} \tilde{n}(\bar{\mathbf{f}} - \bar{\mathbf{g}}) \\ & \times \left(\frac{J_1(|\delta\mathbf{f}/2 + \mathbf{g}|)}{|\delta\mathbf{f}/2 + \mathbf{g}|} \right) \left(\frac{J_1(|\delta\mathbf{f}/2 - \mathbf{g}|)}{|\delta\mathbf{f}/2 - \mathbf{g}|} \right) \end{aligned} \quad (\text{D2})$$

where \tilde{n} is the momentum distribution, as discussed in the main text, and we have normalized by the (homogeneous) density n . The mutual intensity function is best cast in terms of the mean $\bar{\mathbf{f}} = (\mathbf{f}_1 + \mathbf{f}_2)/2$ and difference $\delta\mathbf{f} = \mathbf{f}_1 - \mathbf{f}_2$ of the dimensionless far-field position variables, where $\mathbf{f}_1 = a\bar{k}\mathbf{r}_1/Z$ and $\mathbf{f}_2 = a\bar{k}\mathbf{r}_2/Z$. In the classical Maxwell-Boltzmann limit, we use the Gaussian momentum density $\tilde{n}(\mathbf{k}_\parallel) = e^{-\xi^2 k_\parallel^2/4}$ and the density $n = 1/\lambda_T^2$. Evaluating at $\mathbf{r}_1 = -\mathbf{r}_2 = \mathbf{r}$ or $\bar{\mathbf{f}} = 0$ we

obtain

$$\begin{aligned} \Gamma(\mathbf{0}, 2\mathbf{f}) &= \frac{\pi |A|^2 a^4 \xi_r^2}{\bar{\lambda}^2 Z^2} \int_0^\infty dg \int_0^{2\pi} d\eta g e^{-\xi_r^2 g^2/4} \\ &\times \left(\frac{J_1 \left((f^2 + g^2 + 2fg \cos(\eta))^{1/2} \right)}{(f^2 + g^2 + 2fg \cos(\eta))^{1/2}} \right) \\ &\times \left(\frac{J_1 \left((f^2 + g^2 - 2fg \cos(\eta))^{1/2} \right)}{(f^2 + g^2 - 2fg \cos(\eta))^{1/2}} \right) \end{aligned} \quad (\text{D3})$$

where η is geometrically the angle between \mathbf{f} and \mathbf{g} . Although the expressions look different, the intensity and mutual intensity function are equal on-axis $\mathbf{r} = 0$ with the value

$$\begin{aligned} I(0) = \Gamma(0, 0) &= \frac{\pi^2 |A|^2 a^4 \xi_r^2}{\bar{\lambda}^2 Z^2} \\ &\times \left(1 - e^{-2/\xi_r^2} \left(I_1 \left(\frac{2}{\xi_r^2} \right) + I_0 \left(\frac{2}{\xi_r^2} \right) \right) \right) \end{aligned} \quad (\text{D4})$$

where I_ν is the ν -order modified Bessel function of the first kind.

Next, consider the case of Bose gas correlations. Since the exact mutual intensity function is expressed as a series of Gaussian functions, i.e. Eq. 4, we could apply the Gaussian results to the problem at hand. However, this is computationally intense if the classical coherence length ξ_0 is small compared to the aperture radius a as many nontrivial terms become important for $z \rightarrow 1$. Alternatively, if the classical coherence length ξ_0 is a sufficiently large fraction of the aperture radius a , then there exists $j \geq 1$ not too large such that the diffracted mutual intensity function may be approximated by the analytically known diffraction pattern for a completely coherent source.

But since we are primarily interested in the former case, we instead directly use the Bose-Einstein momentum distribution in Eq. D2. This approach allows us to probe the parameter-space more quickly. We list the simplified propagation integrals here. The intensity is

$$\begin{aligned} I(\mathbf{f}) &= \frac{\epsilon_0 c}{2} \frac{\pi |A|^2 a^4 \xi_{0,r}^2}{\bar{\lambda}^2 Z^2 (-\log(1-z))} \\ &\times \int_0^\infty dg \int_0^{2\pi} d\eta \frac{g}{z^{-1} e^{\xi_{0,r}^2 (f^2 + g^2 - 2fg \cos(\eta))/4} - 1} \\ &\times \left(\frac{J_1(g)}{g} \right)^2 \end{aligned} \quad (\text{D5})$$

where now $\xi_{0,r} = \xi_0/a$ is the classical coherence length relative to the aperture radius. The mutual intensity

function evaluated at $\mathbf{r}_1 = -\mathbf{r}_2 = \mathbf{r}$ or $\bar{\mathbf{f}} = 0$ is

$$\begin{aligned} \Gamma(\mathbf{0}, 2\mathbf{f}) &= \frac{\pi |A|^2 a^4 \xi_{0,r}^2}{\bar{\lambda}^2 Z^2 (-\log(1-z))} \\ &\times \int_0^\infty dg \int_0^{2\pi} d\eta \frac{g}{z^{-1} e^{\xi_{0,r}^2 (f^2 + g^2)/4} - 1} \\ &\times \left(\frac{J_1 \left((f^2 + g^2 + 2fg \cos(\eta))^{1/2} \right)}{(f^2 + g^2 + 2fg \cos(\eta))^{1/2}} \right) \\ &\times \left(\frac{J_1 \left((f^2 + g^2 - 2fg \cos(\eta))^{1/2} \right)}{(f^2 + g^2 - 2fg \cos(\eta))^{1/2}} \right) \end{aligned} \quad (\text{D6})$$

For comparison to experiment, it is more instructive to use the density rather than the fugacity as a parameter. Introducing the particle number in the aperture $\zeta = \pi a^2 n$, we can rewrite the integral expressions for the intensity and mutual intensity function in a non-dimensional form with the substitution $\zeta = -\log(1-z)/\xi_{0,r}^2$ and $z = 1 - e^{-\xi_{0,r}^2 \zeta}$. This is the parameterization used in the main text. With these expressions, the coherent fraction can be calculated numerically.

Appendix E: Coherence function at finite time-separation

Following Ref. [22], the full first-order coherence function as a function of the position separation $r = |\mathbf{r} - \mathbf{r}'|$ and the dimensionless thermal time-separation $\theta = k_B T (t - t')/\hbar$ is

$$G(r, \theta) = \frac{1}{\pi \xi_0^2} \sum_{j=1}^{\infty} \frac{z^j}{j + i\theta} e^{-r^2/\xi_0^2 (j+i\theta)} \quad (\text{E1})$$

which can be normalized by the usual homogeneous density $n = -\log(1-z)/\pi \xi_0^2$ to obtain the normalized full first-order coherence function $g^{(1)}(r, \theta)$. Following Sec. III A, we can calculate the coherent fraction for a classical Maxwell-Boltzmann source $z \rightarrow 0$ over a disk of radius a in the limit of uniform intensity

$$C_{\text{GS}}(\theta) = \frac{\xi^2}{4a^2} \left(1 - e^{-4a^2/\xi^2 (1+\theta^2)} \cos \left(\frac{4\theta}{\xi^2 (1+\theta^2)} \right) \right) \quad (\text{E2})$$

Therefore, the coherent fraction C_{GS} can exhibit oscillations in both the coherence length ξ (with $\theta \neq 0$) and the time-separation θ (with ξ finite). This is in contrast to the correlation area which is more well-behaved

$$\int d^2r \left| g^{(1)}(r, \theta) \right|^2 = \frac{\pi \xi^2}{2} \left(1 - e^{-2a^2/\xi^2 (1+\theta^2)} \right) \quad (\text{E3})$$

In the limit of no aperture $a \rightarrow \infty$ with the coherence length ξ and time-separation θ fixed, the correlation area becomes $\pi \xi^2/2$ which is independent of the time-separation θ as the disk no longer limits which points

can contribute to the correlations. Similarly, the coherence time is

$$\int d\theta \left| g^{(1)}(r=0, \theta) \right|^2 = \pi \quad (\text{E4})$$

which is quoted in the main text.

The coherent fraction at finite time-separations in the case of Bose gas correlations can be defined similarly to Eq. 15

$$C_{\text{BG}}(\theta) = \frac{1}{-\log(1-z)} \sum_{j=1}^{\infty} \frac{z^j}{j} C_{\text{GS}}\left(\frac{\theta}{j}, \sqrt{j}\xi_0\right) \quad (\text{E5})$$

where $C_{\text{GS}}(\theta/j, \sqrt{j}\xi_0)$ denotes the classical Maxwell-Boltzmann result Eq. E2 with the adjusted dimensionless thermal time-separation θ/j and the adjusted coherence length $\sqrt{j}\xi_0$. The expression for $C_{\text{BG}}(\theta)$ does not yield oscillations in the fugacity z or equivalently the density n , a fact which is already clear from Eq. E1.

-
- [1] H. Deng, H. Haug, and Y. Yamamoto, Exciton-polariton Bose-Einstein condensation, *Reviews of Modern Physics* **82**, 1489 (2010).
- [2] V. Timofeev and D. Sanvitto, eds., *Exciton Polaritons in Microcavities: New Frontiers*, Springer Series in Solid-State Sciences, Vol. 172 (Springer Berlin Heidelberg, Berlin, Heidelberg, 2012).
- [3] H. Deng, G. Weihs, C. Santori, J. Bloch, and Y. Yamamoto, Condensation of semiconductor microcavity exciton polaritons, *Science* **298**, 199 (2002).
- [4] J. Kasprzak, M. Richard, S. Kundermann, A. Baas, P. Jeambrun, J. M. J. Keeling, F. M. Marchetti, M. H. Szymańska, R. André, J. L. Staehli, V. Savona, P. B. Littlewood, B. Deveaud, and L. S. Dang, Bose-Einstein condensation of exciton polaritons, *Nature* **443**, 409 (2006).
- [5] H. Deng, D. Press, S. Götzinger, G. S. Solomon, R. Hey, K. H. Ploog, and Y. Yamamoto, Quantum degenerate exciton-polaritons in thermal equilibrium, *Physical Review Letters* **97**, 146402 (2006).
- [6] R. Balili, V. Hartwell, D. Snoke, L. Pfeiffer, and K. West, Bose-Einstein condensation of microcavity polaritons in a trap, *Science* **316**, 1007 (2007).
- [7] P. B. Littlewood, P. R. Eastham, J. M. J. Keeling, F. M. Marchetti, B. D. Simons, and M. H. Szymanska, Models of coherent exciton condensation, *Journal of Physics: Condensed Matter* **16**, S3597 (2004).
- [8] H. Deng, G. S. Solomon, R. Hey, K. H. Ploog, and Y. Yamamoto, Spatial coherence of a polariton condensate, *Physical Review Letters* **99**, 126403 (2007).
- [9] Analogous experiments have been performed in photonic gases [53].
- [10] K. G. Lagoudakis, M. Wouters, M. Richard, A. Baas, I. Carusotto, and R. Andre, Quantized vortices in an exciton-polariton condensate, *Nature Physics Letters* **4**, doi:10.1038/nphys1051 (2008).
- [11] Y. Sun, P. Wen, Y. Yoon, G. Liu, M. Steger, L. N. Pfeiffer, K. West, D. W. Snoke, and K. A. Nelson, Bose-Einstein condensation of long-lifetime polaritons in thermal equilibrium, *Physical Review Letters* **118**, 016602 (2017).
- [12] J. Marelic, L. F. Zajiczek, H. J. Hesten, K. H. Leung, E. Y X Ong, F. Mintert, and R. A. Nyman, Spatiotemporal coherence of non-equilibrium multimode photon condensates, *New Journal of Physics* **18**, 103012 (2016).
- [13] V. L. Berezinskii, Destruction of long-range order in one-dimensional and two-dimensional systems having a continuous symmetry group I. Classical systems, *Soviet Physics JETP* **32**, 493 (1971).
- [14] J. M. Kosterlitz, Ordering, metastability and phase transitions in two-dimensional systems, *Physical Review C* (1973).
- [15] G. Roumpos, M. Lohse, W. H. Nitsche, J. Keeling, M. H. Szymańska, P. B. Littlewood, A. Löffler, S. Höfling, L. Worschech, A. Forchel, and Y. Yamamoto, Power-law decay of the spatial correlation function in exciton-polariton condensates, *Proceedings of the National Academy of Sciences* **109**, 6467 (2012).
- [16] M. Kardar, G. Parisi, and Y.-C. Zhang, Dynamic scaling of growing interfaces, *Physical Review Letters* **56**, 889 (1986).
- [17] O. K. Diessel, S. Diehl, and A. Chiocchetta, Emergent Kardar-Parisi-Zhang phase in quadratically driven condensates, *Physical Review Letters* **128**, 070401 (2022).
- [18] Q. Fontaine, D. Squizzato, F. Baboux, I. Amelio, A. Lemaître, M. Morassi, I. Sagnes, L. Le Gratiet, A. Harouri, M. Wouters, I. Carusotto, A. Amo, M. Richard, A. Minguzzi, L. Canet, S. Ravets, and J. Bloch, Kardar-Parisi-Zhang universality in a one-dimensional polariton condensate, *Nature* **608**, 687 (2022).
- [19] H. Alnatah, Q. Yao, J. Beaumariage, S. Mukherjee, M. C. Tam, Z. Wasilewski, K. West, K. Baldwin, L. N. Pfeiffer, and D. W. Snoke, Coherence measurements of polaritons in thermal equilibrium reveal a power law for two-dimensional condensates, *Science Advances* **10**, eadk6960 (2024).
- [20] M. Naraschewski and R. J. Glauber, Spatial coherence and density correlations of trapped Bose gases, *Physical Review A* **59**, 4595 (1999).
- [21] L. Corman, *The two-dimensional Bose gas in box potentials*, Ph.D. thesis, PLS (2016).
- [22] M. Kohnen and R. A. Nyman, Temporal and spatiotemporal correlation functions for trapped Bose gases, *Physical Review A* **91**, 033612 (2015).
- [23] X. S. Cai and J. L. López, A note on the asymptotic expansion of the Lerch's transcendent, *Integral Transforms and Special Functions* **30**, 844 (2019).
- [24] E. Wolf, *Introduction to the Theory of Coherence and Polarization of Light* (Cambridge University Press, 2007).
- [25] E. Wolf and L. Mandel, *Optical coherence and quantum optics* (Cambridge University Press, 1995).
- [26] G. Gbur and T. Visser, The structure of partially coherent

- ent fields, in *Progress in Optics*, Vol. 55 (Elsevier, 2010) pp. 285–341.
- [27] G. Gbur, T. D. Visser, and E. Wolf, Anomalous behavior of spectra near phase singularities of focused waves, *Physical Review Letters* **88**, 013901 (2001).
- [28] G. Gbur, T. D. Visser, and E. Wolf, Singular behavior of the spectrum in the neighborhood of focus, *Journal of the Optical Society of America A* **19**, 1694 (2002).
- [29] S. A. Ponomarenko and E. Wolf, Spectral anomalies in a Fraunhofer diffraction pattern, *Optics Letters* **27**, 1211 (2002).
- [30] J. W. Goodman, *Fourier Optics*, 2nd ed. (McGraw-Hill, 1968).
- [31] A. C. Schell, *The Multiple Plate Antenna*, Ph.D. thesis, Massachusetts Institute of Technology (1961).
- [32] K. Nugent, A generalization of Schell's theorem, *Optics Communications* **79**, 267 (1990).
- [33] F. Shen and A. Wang, Fast-Fourier-transform based numerical integration method for the Rayleigh-Sommerfeld diffraction formula, *Applied Optics* **45**, 1102 (2006).
- [34] R. A. Shore, B. J. Thompson, and R. E. Whitney, Diffraction by apertures illuminated with partially coherent light, *Journal of the Optical Society of America* **56**, 733 (1966).
- [35] R. A. Shore, Effect of the phase term in the mutual coherence function on aperture-diffraction patterns, *Journal of the Optical Society of America* **58**, 1484 (1968).
- [36] K. Singh and B. N. Gupta, Partially coherent Fraunhofer diffraction by a circular aperture with pupil of non-uniform transmission, *Nouvelle Revue d'Optique Appliquée* **2**, 97 (1971).
- [37] H. F. Schouten, T. D. Visser, and E. Wolf, New effects in Young's interference experiment with partially coherent light, *Optics Letters* **28**, 1182 (2003).
- [38] G. Gbur and T. D. Visser, Young's interference experiment: Past, present, and future, in *Progress in Optics*, Vol. 67 (Elsevier, 2022) pp. 275–343.
- [39] O. Penrose and L. Onsager, Bose-Einstein condensation and liquid helium, *Physical Review* **104**, 576 (1956).
- [40] K. Sakmann, *Many-Body Schrödinger Dynamics of Bose-Einstein Condensates* (Springer Berlin Heidelberg, Berlin, Heidelberg, 2011).
- [41] E. Collett and E. Wolf, Beams generated by Gaussian quasi-homogeneous sources, *Optics Communications* **32**, 27 (1980).
- [42] H. F. Schouten, G. Gbur, T. D. Visser, and E. Wolf, Phase singularities of the coherence functions in Young's interference pattern, *Optics Letters* **28** (2003).
- [43] G. Wachtel, L. M. Sieberer, S. Diehl, and E. Altman, Electrodynamic duality and vortex unbinding in driven-dissipative condensates, *Physical Review B* **94**, 104520 (2016).
- [44] M. Schick, Two-dimensional system of hard-core Bosons, *Physical Review A* **3**, 1067 (1971).
- [45] E. H. Lieb, R. Seiringer, and J. Yngvason, A rigorous derivation of the Gross-Pitaevskii energy functional for a two-dimensional Bose gas, *Communications in Mathematical Physics* **224**, 17 (2001).
- [46] A. Posazhennikova, Colloquium: Weakly interacting, dilute Bose gases in 2D, *Reviews of Modern Physics* **78**, 1111 (2006).
- [47] F. M. Marchetti, J. Keeling, M. H. Szymańska, and P. B. Littlewood, Absorption, photoluminescence, and resonant Rayleigh scattering probes of condensed microcavity polaritons, *Physical Review B* **76**, 115326 (2007).
- [48] F. M. Marchetti, M. H. Szymańska, J. M. J. Keeling, J. Kasprzak, R. André, P. B. Littlewood, and L. Si Dang, Phase diagram for condensation of microcavity polaritons: From theory to practice, *Physical Review B* **77**, 235313 (2008).
- [49] P. C. Hohenberg and P. C. Martin, Microscopic theory of superfluid helium, *Annals of Physics* **34**, 291 (1965).
- [50] Z. Hadzibabic and J. Dalibard, Two-dimensional Bose fluids: An atomic physics perspective, *La Rivista del Nuovo Cimento* **34**, 389 (2011).
- [51] R. Saint-Jalm, *Exploring two-dimensional physics with Bose gases in box potentials: phase ordering and dynamical symmetry*, Ph.D. thesis, PLS (2019).
- [52] C. W. Helstrom, Detection and resolution of incoherent objects seen through a turbulent medium, *Journal of the Optical Society of America* **59**, 331 (1969).
- [53] T. Damm, D. Dung, F. Vewinger, M. Weitz, and J. Schmitt, First-order spatial coherence measurements in a thermalized two-dimensional photonic quantum gas, *Nature Communications* **8**, 158 (2017).